Atmospheric Sensitivity to SST near the Kuroshio Extension during the Extratropical Transition of Typhoon Tokage*

NICHOLAS A. BOND

Joint Institute for the Study of the Atmosphere and Ocean, University of Washington, Seattle, Washington

MEGHAN F. CRONIN

NOAA/Pacific Marine Environmental Laboratory, Seattle, Washington

MATTHEW GARVERT

3Tier, Seattle, Washington

(Manuscript received 19 August 2009, in final form 30 January 2010)

ABSTRACT

It is hypothesized that the tropical-to-extratropical transition of a cyclone in the western North Pacific can be sensitive to the underlying sea surface temperature (SST) distribution. This hypothesis was tested through a case study of Typhoon Tokage using a series of high-resolution simulations by the Weather Research Forecast (WRF) numerical weather prediction model. Simulations were carried out for a control SST distribution and for SST distributions with imposed warm and cold perturbations of 1.5°C maximum amplitude in the vicinity of the Kuroshio Extension. The simulations with the warm SST perturbation yielded a cyclone slightly weaker than in the control SST case about 2 days after transition. In contrast, the cold SST perturbation case yielded a cyclone with a central pressure 10 hPa lower than in the control case at the same point in the storm's life cycle, apparently due to its more northward track and hence closer proximity to an approaching upper-level trough and perhaps in association with a stronger warm front. The effects of the regional SST on the simulated storms are manifested not just locally, but also cause substantial impacts on 500-hPa geopotential heights over much of the North Pacific basin. Retrospective analysis of meridional heat fluxes associated with these events using the NCEP–NCAR reanalysis was carried out for early fall (September–November) seasons with relatively warm and cool SST in the region of the imposed SST perturbations. Differences in the patterns of these fluxes between the warm and cool years are broadly consistent with the results from the warm versus cool SST simulations for Typhoon Tokage.

1. Introduction

Tropical cyclones are common in the western North Pacific during late summer and early fall (Chan 2005), and many of them include a northward track over the Kuroshio Extension east of Japan. At this stage in their life cycle, these cyclones typically undergo a transition from a symmetric, warm-core to a baroclinic, cold-core structure. Such a transition can be accompanied by either decay or reintensification of the surface cyclone, depending on the interactions between the remnant cyclonic circulation and the midlatitude conditions that it encounters (e.g., Hart et al. 2006). We hypothesize that these interactions can be influenced by the underlying sea surface temperature (SST) distribution through the latter's effect on lower-tropospheric thermodynamic properties prior to and during cyclone passage. While there is a clear local atmospheric response to the marked meridional gradient in SST associated with western boundary currents (Nakamura et al. 2004; Tokinaga et al. 2006; Minobe et al. 2008; Tokinaga et al. 2009), the extent to which the larger-scale atmospheric circulation is sensitive to anomalies in SST is controversial (e.g., Kushnir et al. 2002). There is tentative evidence that this sensitivity is mediated by the atmosphere's basic

* Joint Institute for the Study of the Atmosphere and Ocean Contribution Number 1768 and Pacific Marine Environmental Laboratory Contribution Number 3425.

Corresponding author address: Nicholas A. Bond, JISAO, University of Washington, Box 354925, Seattle, WA 98195-4925.
E-mail: nab3met@u.washington.edu

DOI: 10.1175/2010MWR3198.1

© 2010 American Meteorological Society

state (e.g., Peng et al. 1997; Bond and Harrison 2000). It is plausible to suppose that extratropical transitions are particularly sensitive to SST, because of the latter's impact on the surface fluxes of sensible and latent heat, which themselves represent the primary energy source for tropical cyclones (e.g., Emanuel 1986). One might expect that anomalously warm SSTs would tend to be associated with delayed transitions for storms moving poleward, and that cold SSTs would be associated with hastened transitions, all other factors being equal. Thus, the effects of the regional SST on these storms may not have just local manifestations. Modifications in storm properties have potential impacts on the atmospheric circulation over the entire North Pacific basin through the downstream propagation of eddy activity/wave energy (e.g., Chang and Orlanski 1993).

The present contribution on the subject of tropical to extratropical cyclone transition, and in particular the role of the ocean, is based on a series of high-resolution numerical weather prediction (NWP) model simulations of a single storm, Typhoon Tokage in October 2004. This case was selected because of the previous work carried out by Anwender et al. (2008) and Torn and Hakim (2009). The former study investigated the downstream predictability using the European Centre for Medium-Range Weather Forecasts (ECMWF) ensemble prediction system; the latter study used an ensemble of NWP model simulations to explore the sensitivity of the modeled storm to initial conditions during the early portion of its extratropical phase. The standard deviations in 500-hPa geopotential height from these studies, in the vicinity of Tokage and downstream, provide a standard for comparison with the results from our numerical experiments involving control and perturbed SST distributions.

Our primary simulations are of the impacts of positive and negative perturbations in SST on the relatively broad spatial scale of about 8° latitude and 16° longitude over a region extending from the Sea of Japan eastward to the Kuroshio Extension. Striking differences were found between the post-transition evolution of Tokage in these simulations. We also carried out numerical experiments for which the magnitude of the SST front at the Kuroshio Extension is enhanced and lessened, with no overall change in SST in terms of a spatial average; these results are just briefly summarized. The period of interest is the end of the transition phase through the first few days of the storm's extratropical phase. The simulations were carried out with the Advanced Research Weather and Research Forecasting (WRF 3.0) model (Skamarock et al. 2008) with 15-km grid spacing on an inner nest covering most the western North Pacific Ocean. A retrospective analysis of western North Pacific extratropical transitions based on reanalysis data was carried out to complement the numerical experiments.

The paper is organized as follows. The methodology used in our model experiments is described in the next section. We then provide a brief synoptic review of Tokage, focusing on a 2-day period immediately after its transition. Our principal results are presented in section 4 and consist of material from the control, warm, and cool SST perturbation numerical experiments. The observational analysis of past western North Pacific transitions is the subject of section 5. The final section consists of a summary and discussion.

2. Model experiments

Our analysis is based on WRF 3.0 simulations initialized on 13 October 2004 using the National Centers for Environmental Prediction (NCEP) Global Forecast System (GFS), which also provided lateral boundary conditions throughout the simulations. We focus on the period of 20–22 October, which for Tokage represents the end of the transition phase through the beginning of the extratropical phase. These simulations were carried out with an outer domain with a grid spacing of 45 km, which provided lateral boundary conditions for an inner domain with a grid spacing of 15 km using 1-way nesting. The inner nest extends from about 50° to 10°N and from about 105°E to a portion of the west coast of North America (i.e., nearly the entire North Pacific). We used such a large domain for the inner nest (Fig. 1) in order to resolve the mesoscale structure of the cyclone during both its tropical and extratropical phases. Nudging to the operational initializations from NCEP's GFS was applied on both the outer and inner domains through the first 144 h of the simulations (through 0000 UTC 19 October). For the remaining 7 days of the simulations nudging was applied only on the outer domain, which extended farther than the inner domain by 135 km on each side. We employed a basic set of parameterizations: the Yonsei University (YSU) planetary boundary layer option, the Rapid Radiative Transfer Model (RRTM; longwave) and Dudhia (shortwave) radiation packages, the Ferrier cloud microphysics scheme, and Kain–Fritsch for subgrid-scale cumulus convection. By way of comparison, except for the cloud microphysics, Davis et al. (2008) used a similar set of parameterizations in their WRF simulations of landfalling hurricanes. The SST distribution used for the control experiment is from the Advanced Microwave Scanning Radiometer for Earth Observing System (AMSR-E) dataset valid at 13 October 2004 (Fig. 1). The warm and cool perturbation SST experiments use the control SST distribution and impose SST anomalies with maximum perturbations of 1.5°C at 35°N, 140°W,

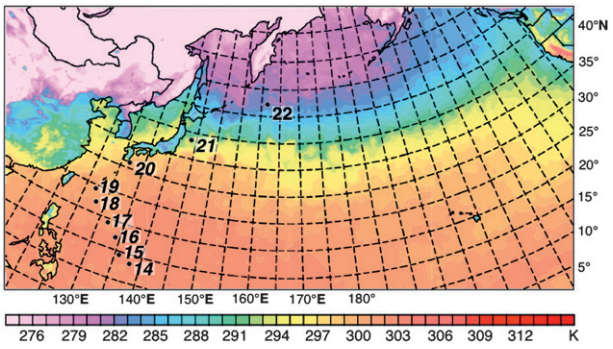

FIG. 1. SST distribution for the control simulation. The region shown represents the domain for the inner nest of the WRF simulations. The locations of the surface low pressure center of Tokage at 0000 UTC from the JTWC are also indicated.

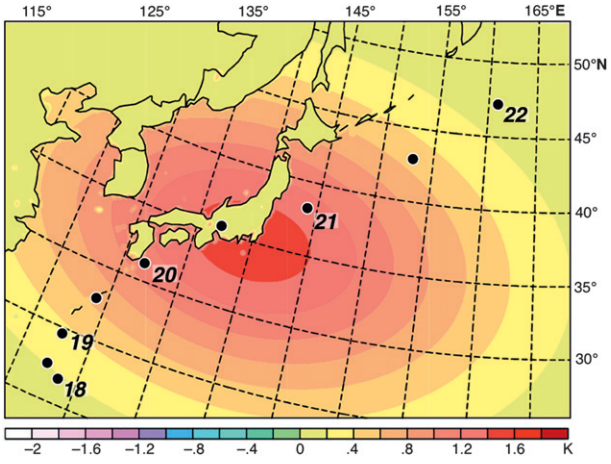

FIG. 2. Perturbation imposed for the warm SST simulation. The locations of Tokage at 12-h intervals from the JTWC are also indicated (numbered dots are dates at 0000 UTC October 2004).

tapering off to background values in a Gaussian manner with *e*-folding scales of 8° in latitude and 16° in longitude (Fig. 2). The shape and magnitude of these SST perturbations resemble the pattern observed during September–November of 1999–2002, when SSTs were relatively warm in the western North Pacific. It is also similar to the distribution of SST anomalies in the western North Pacific associated with the Pacific decadal oscillation (PDO; Mantua et al. 1997), with positive values in negative phases of the PDO and vice versa. The SST perturbations are maintained through the entire duration of the numerical simulations. We focus here on the differences in the modeled atmospheric structure between the control and the positive and negative perturbation SST runs.

3. Synoptic review

The disturbance that became Tokage was first identified by the Joint Tropical Warning Center (JTWC) as a tropical depression at 7°N, 157°E on 10 October 2004. Tokage gained typhoon status on 13 October and reached its maximum (category 4 on the Saffir–Simpson scale) strength on 17 October with a central pressure of 916 hPa and sustained winds of 125 kt. It made landfall in Japan on 20 October on the south side of the island of Shikoku (Fig. 3a) and moved northeast across the central portion of the island of Honshu before moving offshore early on 21 October, at which point the JTWC no longer considered it to be a tropical disturbance. In the cyclone phase space framework of Hart (2003), the indices for the thermal asymmetry (B), lower-tropospheric thermal wind ($-V_T^L$), and upper-tropospheric thermal wind ($-V_T^U$) in the vicinity of Tokage at 0000 UTC 20 October were about 30, −80, and 30, respectively, and at 0000 UTC 21 October were about 60, −280, and −250, respectively. These values indicate that transition was under way at the earlier time and essentially complete by the later time (Evans and Hart 2003). While the post-transition evolution is the focus of the present study, it is noteworthy that Tokage caused the highest number of casualties (including at least 93 deaths; see http://www.unep.or.jp/ietc/wcdr/unep-tokage-report.pdf) for a typhoon striking Japan since 1979.

The cyclone that had been Tokage retained considerable strength as it moved northeast and gained increasingly extratropical characteristics. At 0000 UTC 22 October, it was located at 47°N, 161°E and had a central pressure of 990 hPa (Fig. 3b). The low-level flow in the vicinity of the storm at this time featured strong southwesterly winds in a band greater than 2000 km in length extending from south to northeast of the low pressure center. Its central pressure remained roughly constant over the next 18 h as it continued toward the northeast, and then decreased to a minimum of 977 hPa on 23 October over the Bering Sea. Based on the classification scheme of Klein et al. (2000), Tokage was slightly stronger than average at the end of its transition, but remained of approximately constant strength over the next 2 days. In contrast, most western North Pacific tropical cyclones that survive transition undergo reintensification.

We have examined the regional tropospheric circulation in the vicinity of Tokage in the context of the review of extratropical transitions of Jones et al. (2003), and the case study of Typhoons David and Opal by Harr and Elsberry (2000). The axis of a broad midlatitude 500-hPa trough was near 120°E at 0000 UTC 21 October (Fig. 4) as Tokage was completing its extratropical transition, but this feature was on the order of 1500 km west of Tokage, and does not appear to have been close enough to have had a direct influence at this point in Tokage's evolution. Instead, this trough appears to be associated with the

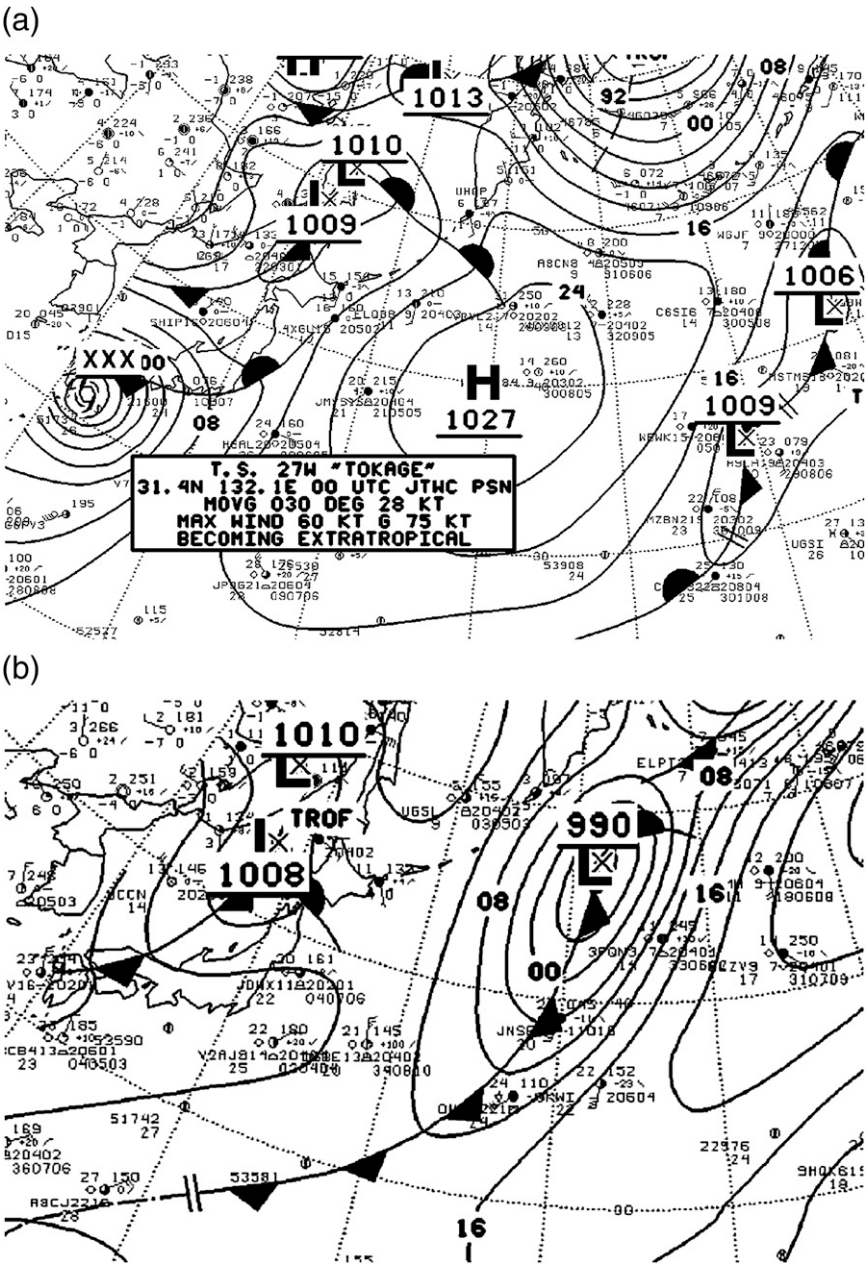

FIG. 3. NCEP–OPC Pacific Ocean surface analysis at (a) 0000 UTC 20 Oct and (b) 0000 UTC 22 Oct 2004.

development of a separate cyclone in the far northern portion of the Sea of Japan. It was also present in our simulations, and as will be discussed later, it likely did play a role in the cyclogenesis found in one of our simulations. Based on the overall pattern of the tropospheric circulation and the maintenance if not strengthening of Tokage's intensity in its extratropical phase, the synoptic setting for cyclogenesis after transition can be characterized as somewhere in between the favorable environment associated with David and the unfavorable environment encountered by Opal (Harr and Elsberry 2000). Additional information on Tokage's evolution is also provided by Torn and Hakim (2009); their ensemble simulations reveal that it is a case in which development in the post-transition phase was relatively sensitive to the upstream flow aloft. A key point for the present study is that during the end of the period of Tokage's tropical phase, and in the early portion of its extratropical phase, the storm's track over the ocean was in the region where SST perturbations were imposed for our NWP model simulations.

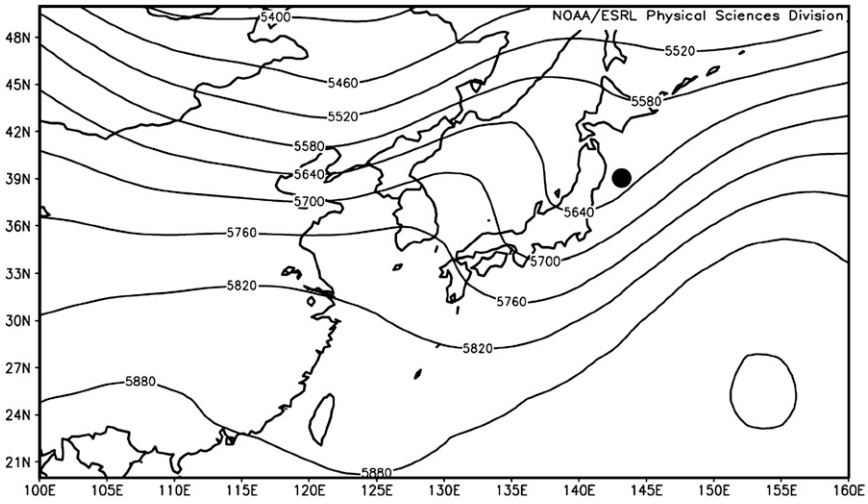

FIG. 4. Geopotential height at 500 hPa (contour interval 60 m) at 0000 UTC 21 Oct 2004 from the NCEP–NCAR reanalysis. The solid dot refers to the approximate location of the surface low center.

4. Warm and cool SST experiments

We begin by reviewing the control WRF simulation with the unperturbed SST as a lower boundary condition. The SLP forecast at 0000 UTC 20 October (Fig. 5a) compares favorably with the observed SLP at the same time shown above. The simulation has the low pressure center located near 31°N, 131°E, within 50–100 km of the observed location. In addition, the simulation yielded a trough of lower SLP and low-level baroclinity extending northeast from the storm center along the east coast of Japan, as shown in the corresponding NCEP analysis (Fig. 3a). The central pressure of the simulated storm at this time is 984 hPa, as compared with the estimate of 976 hPa from JTWC for the actual storm. This discrepancy is not surprising in that even the 15-km grid spacing of the inner nest for our WRF simulation cannot be expected to resolve the inner core of a tropical cyclone. That being said, we contend that the control WRF simulation of Tokage through its tropical phase is impressive, especially considering that the map shown in Fig. 5a represents the solution 7 days into the simulation.

The control simulation of SLP 2 days later at 0000 UTC 22 October (Fig. 5b) indicates a low pressure center of 993 hPa located near 43°N, 154°E representing Tokage after transition. The intensity of the simulated storm is close to that of the observed storm, at least as gauged by the estimated central pressure of 990 hPa from the NCEP analysis (Fig. 3b). The control simulation has the center of the storm southwest of its analyzed position, but the overall SLP pattern of an elongated trough extending from southwest to northeast of the storm center is indicated in both the simulation and the NCEP analysis. In particular, both the simulation and the analysis show a pressure pattern supporting a band of relatively strong southwesterly low-level flow ahead of the storm. Our interpretation of the control simulation is that it replicated the end of the tropical phase of Tokage, its transition, and the first 2 days of its evolution after transition, to a realistic enough degree that our other simulations yield meaningful measures of the sensitivities of this storm to the underlying SST.

The SLP distributions at 0000 UTC 20 October and 0000 UTC 22 October from the WRF simulation incorporating the warm SST perturbation are shown in Figs. 6a,b, respectively. For the earlier time, this simulation yielded a position for Tokage virtually identical to that from the control simulation, and a central pressure that is 2 hPa lower. Perhaps this similarity between the two simulations is to be expected in that up until this point in its history, the track of Tokage was well south of the axis of the maximum in the prescribed SST perturbations. What may represent more of a surprise is the result for two days later, after Tokage crossed the Kuroshio Extension and the region of perturbed SST. At this time, the simulated SLP minimum is 200 km southeast of its counterpart in the control simulation, and its magnitude is 996 hPa, which is actually about 3 hPa higher than in the control simulation. The 925-hPa air temperatures in the vicinity of the storm center, and in the storm's warm sector, are about 1°C greater in this simulation than in the control. By this measure, the storm in the warm SST simulation retained tropical characteristics a bit longer than the storm in the control simulation. On the other hand, the temperature gradients in the warm sector east of 160°E from about 40°–45°N are also slightly greater in

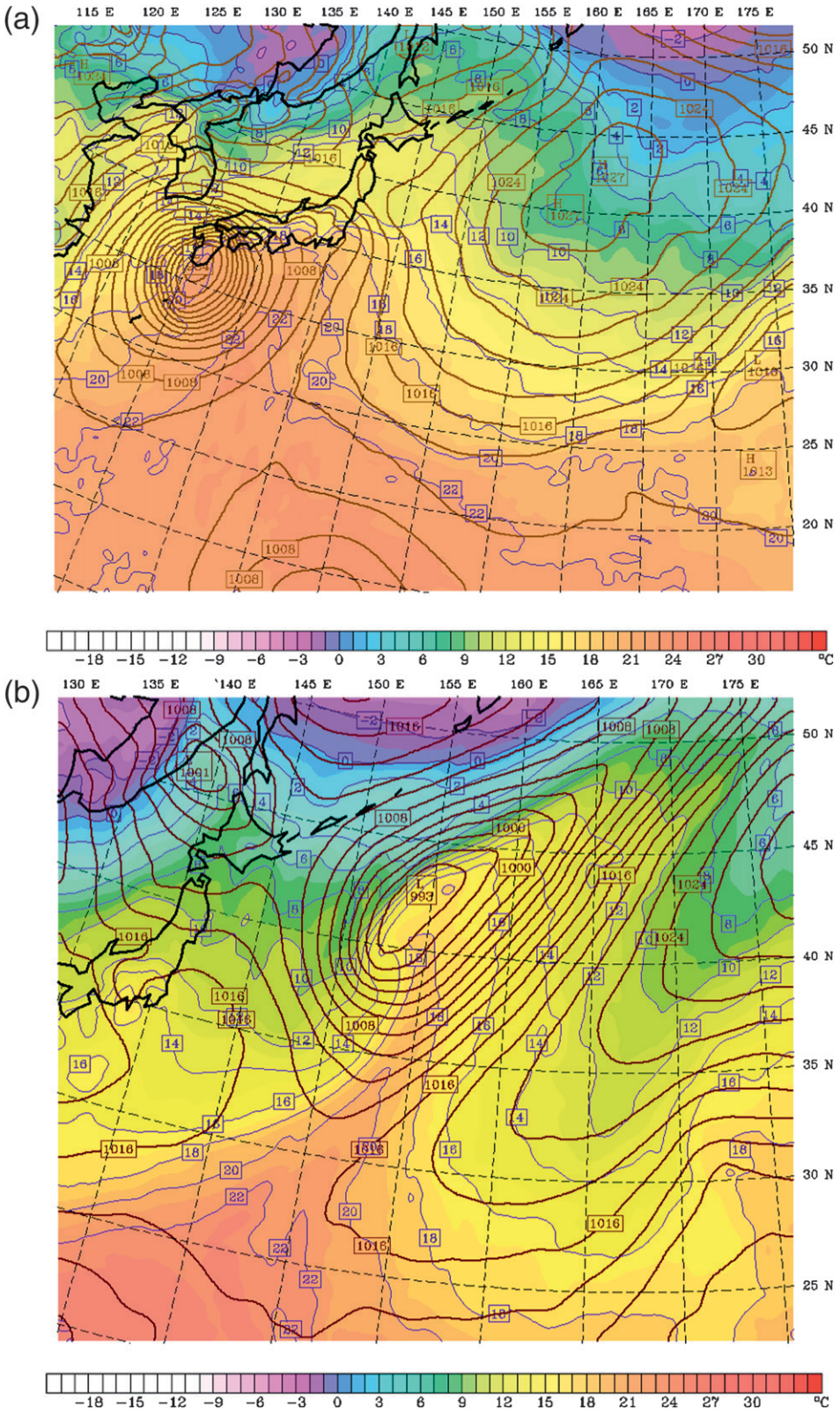

FIG. 5. Sea level pressure (brown solid lines; contour interval 2 hPa) and 925-hPa air temperatures (thin blue lines every 2°C with color fills) from the control SST simulation at (a) 0000 UTC 20 Oct and (b) 0000 UTC 22 Oct 2004.

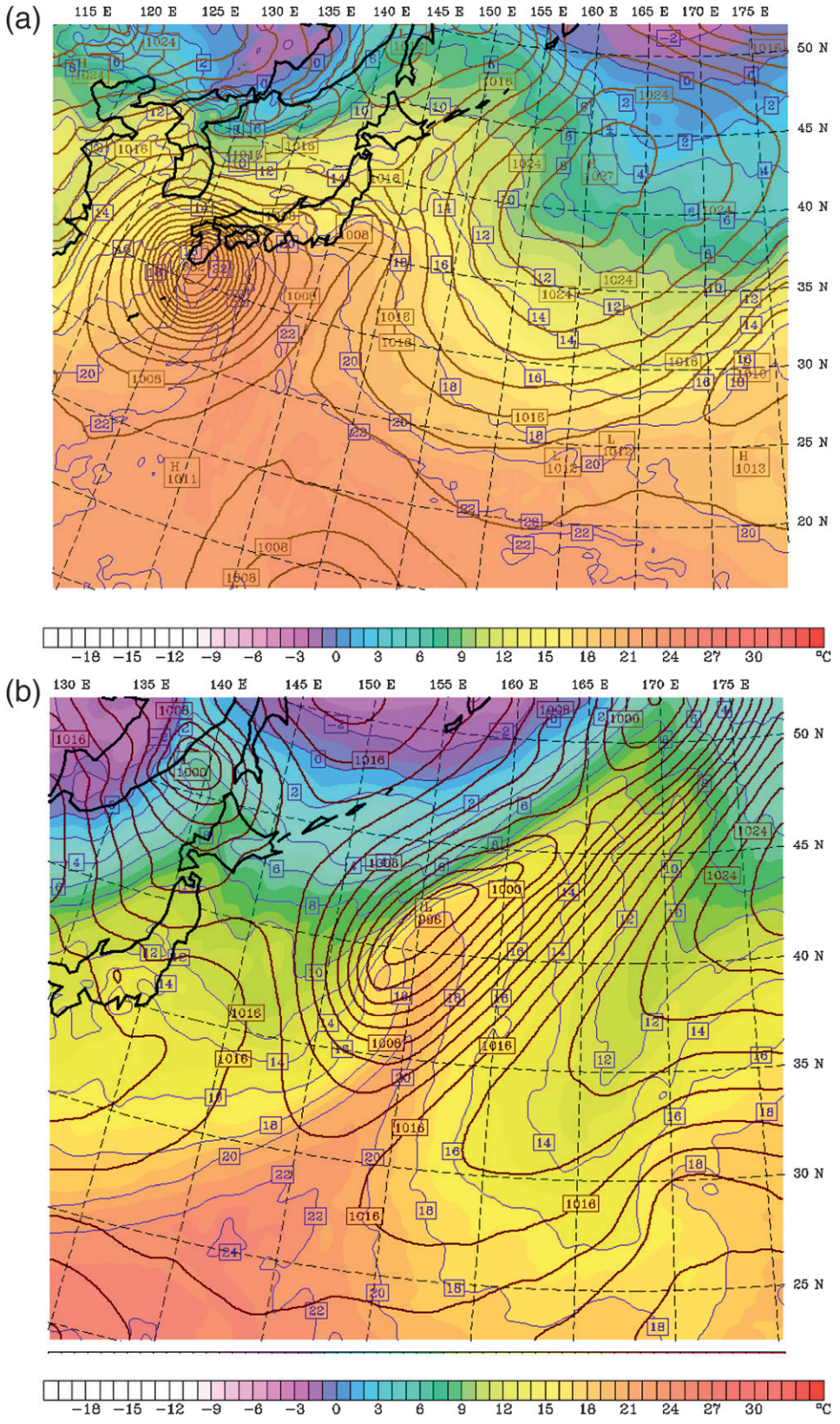

FIG. 6. As in Fig. 5, but for the warm SST perturbation simulation.

this simulation, implying greater low-level warm advection ahead of the storm relative to the control simulation. In the cyclone phase space of Hart (2003), the thickness asymmetry parameter B was about 12 m larger in the warm SST perturbation than in the control simulation by 22 October.

The simulation for which the cool SST was prescribed reveals a decidedly different evolution for Tokage after transition. The SLP map for 0000 UTC 20 October (Fig. 7a) indicates a location for Tokage that is very close to that found in the control and warm SST simulations, and a central pressure about 3 hPa higher. Evidently, the effects of the SST perturbations during Tokage's tropical phase are modest and quasi-linear, with warm (cool) SST resulting in a slightly stronger (weaker) storm at landfall in southern Japan. In contrast, Tokage actually gains strength after transition in the cool SST simulation, unlike in the control and warm SST simulations. The cool SST simulation yielded a central pressure of 983 hPa for Tokage at 0000 UTC 22 October (Fig. 7b), which is about 10 hPa lower than in the control simulation. The low pressure center is located near 44°N, 152°E, which is about 300 km northwest of the center in the control simulation. This difference in its track resulted in the surface low center being closer to an upper-tropospheric trough approaching from the west off the continent of Asia (observed counterpart shown in Fig. 4). It apparently represented a considerably more favorable environment for cyclogenesis. This result is consistent with Hart et al. (2006), which showed that the separation between the upper-level trough and the low-level center was systematically less for the cases with strengthening in the post-transition phase than for those with weakening. It is also consistent with the simulations of Torn and Hakim (2009) who found that Tokage's minimum SLP after transition was sensitive to both the position of the surface low center and the approaching midlatitude trough, and hence their interactions.

The distribution of 925-hPa air temperature in Fig. 7b from the cool SST simulation reveals a much more prominent warm front than in the other two simulations. This difference can be attributed to the track of the storm, which is more toward the colder air to the north, the enhanced development of the storm itself, and, as addressed further below, to the distribution of low-level surface heat fluxes during the past day or so relative to those in the other simulations. In turn, the strength of the warm front had implications for cyclogenesis through the self-development mechanism of Sutcliffe and Forsdyke (1950). This mechanism was discussed by Bosart and Lackmann (1995) regarding Hurricane David's transition in the North Atlantic. In brief, the stronger warm front in the cool simulation versus the more prominent warm advection well east of the storm center in the other simulations, implies greater geopotential height rises immediately east of the low center. This causes both a shift to the left in the track of the storm, and a more favorable environment for cyclogenesis due to enhanced positive vorticity advection with the approaching upper-level trough. Assuming that the track of the storm, and presumably, also the nature of the low-level warm advection in its advance, are crucial to its development, we now consider why these differed in our simulations.

The only changes that were externally imposed in our numerical experiments were to the SST, and it is worthwhile to examine how these changes were communicated to the atmosphere through the fluxes of sensible and latent heat at the air–sea interface. As mentioned earlier, the SST perturbations were imposed for the duration of the experiments, and so their impacts include the periods before and after the passage of Tokage itself. It is impractical to show the full history of the surface heat fluxes, and so for brevity's sake, here we illustrate the effects of the imposed SST perturbations on these fluxes through a set of maps for the single time of 0000 UTC 21 October. This time was chosen because while all three simulations had SLP minimums of 990 hPa located near 35°N, 138°E for this time, there were emerging differences in the flow aloft. The distributions of the sum of the surface sensible and latent heat fluxes from the control (Fig. 8), warm SST (Fig. 9), and cool SST (Fig. 10) simulations at 0000 UTC 21 October all feature maximum values south of Japan in the relatively, cool dry low-level northwesterly flow wrapping around the storm center. The warm and cool SST simulations indicate fluxes as great as $\sim$200 W m^{-2} more and less than the control simulation, respectively. However, from the point of view of Tokage's evolution we expect greater sensitivity to the fluxes in the poleward flow east of the surface low center south of the axis of the Kuroshio Extension between roughly 140° and 145°E (region A in Figs. 8–10). The warm and cool SST simulations include fluxes that were $\sim$100 W m^{-2} greater and smaller than in the control simulation, which meant corresponding changes in the meridional gradient in the fluxes across the axis of the Kuroshio Extension along 35°–36°N. The result is greater low-level baroclinicity in the warm SST case with higher thicknesses to the south. An important consequence is shown below. The difference in the heating due to the imposed SST perturbations in this location had been operating for some time; note that the meridional gradients in 925-hPa air temperature in this region at 0000 UTC 20 October for the warm SST case (Fig. 6a) are greater than those for the cool SST case (Fig. 7a). There is also substantially more heating over the Sea of Japan in the warm versus cool SST simulation.

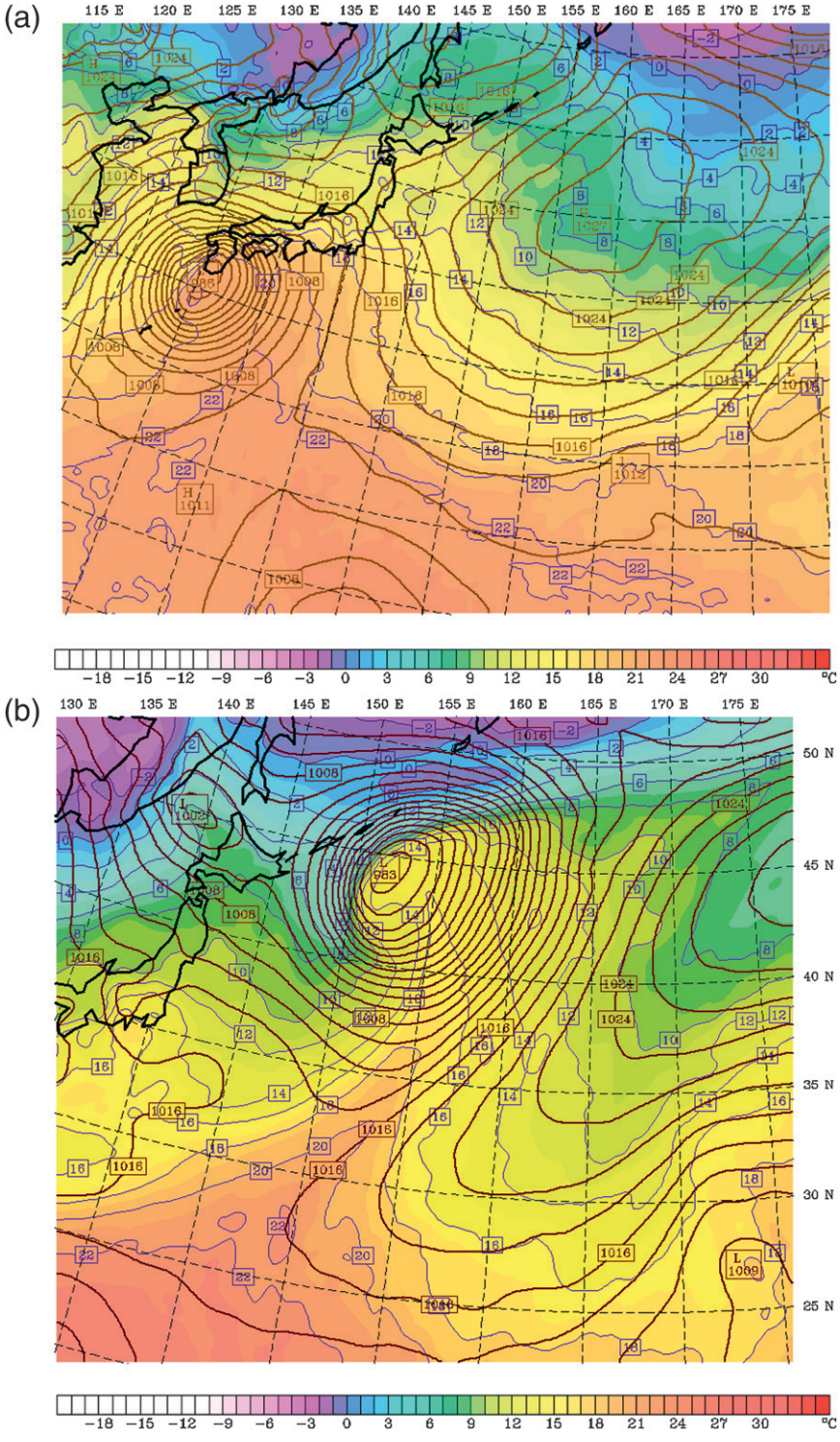

FIG. 7. As in Fig. 5, but for the cool SST perturbation simulation.

The prescribed perturbations in SST have smaller impacts on the combined fluxes in the poleward low-level flow ahead of the storm over the cooler SST north of the Kuroshio. This air originated at lower latitudes and therefore is already relatively warm and moist. It is less influenced by the underlying SST in that the stable surface layer stratification associated with warm air flowing over cooler water effectively helps decouple the atmosphere

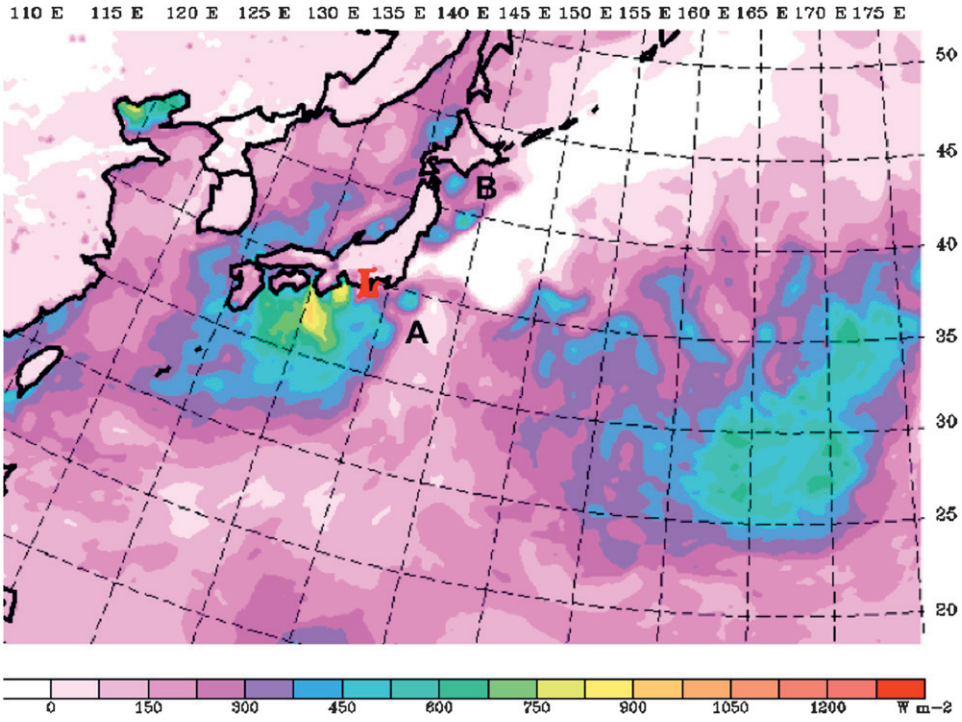

FIG. 8. Sum of sensible and latent heat fluxes (W m^{-2}; color scale at bottom) at 0000 UTC 21 Oct 2004 from the control simulation. The "L" indicates the position of the surface low; the "A" and "B" indicate regions referred to in the text.

from the ocean (e.g., Nonaka and Xie 2003). In other words, SST perturbations in conditions of warm air over cool water will be of less importance than SST perturbations in conditions of cold air over warm water, given other factors being equal. Note that air of 14°C at 925 hPa extends just past 45°N in the warm sectors of the storms at 0000 UTC 22 October in all three simulations (Figs. 5b, 6b, and 7b).

There do appear to be some important differences in the heat fluxes over the cooler water, in the easterlies north of the warm front (region B in Figs. 8–10). The surface fluxes into this relatively cool air are 100–200 W m^{-2} greater in the warm SST than in the cool SST simulation during the 24-h period beginning at 0000 UTC 21 October. In this manner the surface fluxes serve to reduce the strength of the warm front to a greater extent in the warm SST than in the cool SST simulation. As discussed above, this would have feedbacks on the track of the storm through the self-development mechanism, and ultimately the propensity for continued strengthening in its extratropical phase.

The different distributions of surface fluxes are manifested aloft. In particular, the 700-hPa zonal wind from the warm SST simulation at 0000 UTC 21 October (Fig. 11) includes a local maximum of 26 m s^{-1} southeast of the surface low center and a secondary maximum of similar amplitude near 42°N, 150°E. Its counterpart from the cold SST simulation (Fig. 12) includes a maximum to the southeast of the surface low center that is about 2 m s^{-1} less in amplitude, and lacks the additional maximum to the northeast. Especially in the vicinity of Tokage itself, the distinctions between the 700-hPa flow in the two simulations are subtle, but to the extent that this flow represents a steering current for Tokage, there is the indication of a more eastward track away from the eastern coast of Japan in the warm SST simulation (Fig. 11) than in the cool SST simulation (Fig. 12). There is also a difference in the 700-hPa flow over the eastern portion of the Japan Sea; here the warm SST simulation features easterlies that are about 2 m s^{-1} less than those in the cool SST simulation. The overall northwest–southeast asymmetry across the 700-hPa trough in the vicinity of Tokage is slightly greater in the warm SST simulation than in the cool SST simulation.

The differences between the warm and cool SST perturbation simulations can be examined further in terms of the lower-tropospheric baroclinicity. Its distribution, in terms of the vertical wind shear from the surface to the 4-km level, at 0000 UTC 21 October from the warm SST simulation (Fig. 13, top) indicates a prominent band of large wind shear extending northeastward off the eastern coast of Japan, representing the transition zone separating the warm, southwesterly flow to the east of Tokage

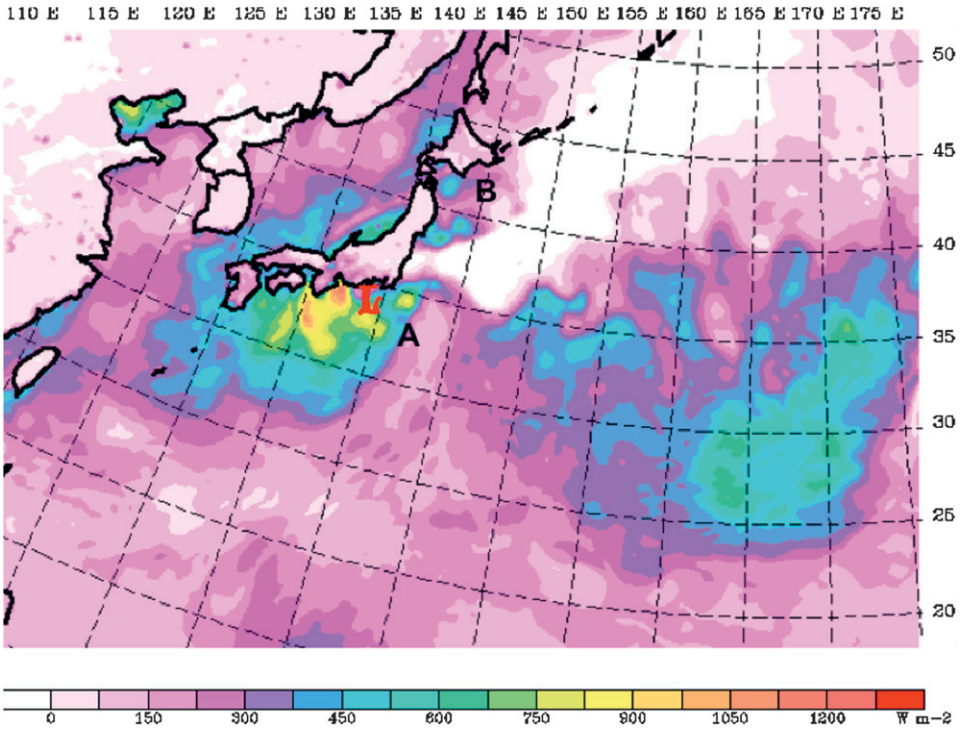

FIG. 9. As in Fig. 8, but for the warm SST perturbation simulation.

from the cold, low-level northeasterly flow to its north. Note also the region of enhanced shear farther east centered near 43°N, 155°E. In the next 12 h (Fig. 13, bottom), the vertical shear associated with Tokage decreases, as its central pressure rose 3 hPa (not shown). The baroclinity to the northeast of Tokage becomes organized into a comma shape near 47°N, 163°E; this secondary development (12 h later) yielded the 998-hPa SLP low center at 52°N, 170°E shown in Fig. 6b. The lower-tropospheric vertical wind shear distribution from the cool SST perturbation simulation valid at 0000 UTC 21 October (Fig. 14, top) reveals slightly more baroclinicity due east of Tokage but actually a lesser magnitude in the primary band of baroclinicity extending off the eastern coast of Japan.

From the perspective of the cyclone phase space of Hart (2003), the timing of the onset of transition, as categorized by the development of low-level thermal asymmetry, is essentially the same in the warm and cool SST simulations. Similarly, the baroclinic growth rate, which is proportional to the vertical wind shear and inversely proportional to the Brunt–Väisälä frequency (e.g., Hart and Evans 2001), is about the same in the two simulations (not shown). On the other hand, the cool SST simulation lacks the secondary storm development to the northeast, as is evident from comparing the vertical wind shear at 1200 UTC 21 October (Fig. 14, bottom) with its counterpart from the warm SST simulation. The upshot is the deepening of a single low pressure center in the cool SST case (7 hPa over the 24-h interval ending at 0000 UTC 22 October) as compared with a filling of 6 hPa of the main center, and the development of an additional low center to the northeast in the warm SST case.

In summary, the simulations with prescribed warm and cool SST perturbations yielded different outcomes for Tokage in the early stage of its extratropical phase. These perturbations, through the surface fluxes of sensible and latent heat, impact the evolution of Tokage (i.e., the dynamics) in a complicated way. For example, from the perspective of the quasigeostrophic geopotential height tendency equation, the fluxes have both direct and indirect effects. In the region of upper-level height falls to the west of the surface center, the differential heating in the warm SST case directly counteract the height falls to a greater extent than in the cool SST case. Conversely, the region of upper-level height rises ahead of the storm features greater differences in the horizontal temperature advection, which are due more to changes in the track of the storm rather than the fluxes themselves. Considering the framework developed by Hart et al. (2006), there is the tendency for increased SST gradients for cases of post-transition strengthening versus weakening. In the present case, however, the meridional gradient in SST north of 35°N (the environment in which the

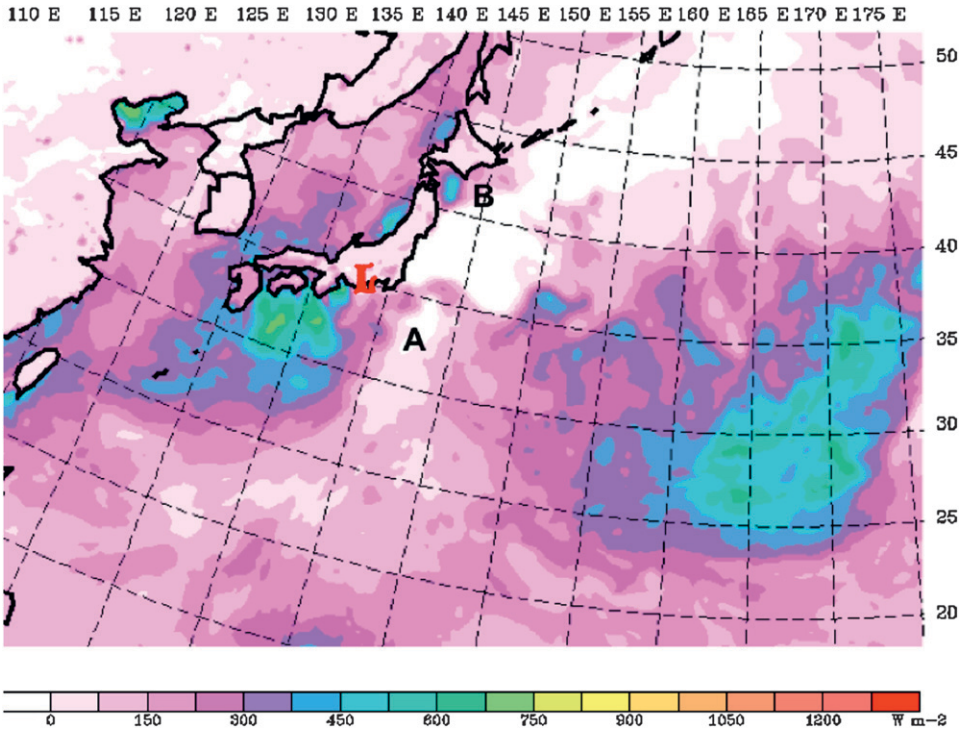

FIG. 10. As in Fig. 8, but for the cool SST perturbation simulation.

evolutions of our simulated storms started diverging significantly) is actually greatest in the warm SST case, which yielded the weakest storm. In addition, the overall environment for cyclogenesis early during Tokage's transition, as characterized by the lower-tropospheric vertical wind shear, is similar in all simulations. On the other hand, the separation distance between the surface cyclone and an approaching upper-tropospheric trough did start becoming different about 24 h into transition (~0000 UTC 21 October), with the cool SST case featuring a smaller separation and greater development, which is consistent with Hart et al. (2006). These differences in the track of Tokage and its morphology are initially slight, but grew rapidly over the course of a day. The changes in the lower-tropospheric thermodynamic properties induced directly by the SST perturbations are augmented by feedbacks with the flow aloft, which evolve differently in the various simulations due to the internal storm dynamics. The bottom line is that the atmosphere ends up being quite sensitive to the SST during this particular instance of an extratropical transition.

Our simulations indicate that the effects of the prescribed SST perturbations have remote impacts as well as in the vicinity of Tokage itself. A map of the 500-hPa geopotential height from the warm SST simulation valid at 0000 UTC 23 October and its deviation from the control simulation in a control minus warm SST sense are shown in Fig. 15. The heights are about 60 m higher than in the control simulation for a small area southeast of the Kamchatka Peninsula in the vicinity of the surface low. Farther downstream, this simulation produced negative perturbations in the 500-hPa heights of as much as 75 m over the eastern Bering Sea and of about 30 m off the coast of the Pacific Northwest. The corresponding map for the cool SST simulation (Fig. 16) is not the mirror image of that for the warm SST case. In particular, the 500-hPa response is generally larger (exceeding 100 m in certain locations) in the cool SST case, especially upstream in the vicinity of the prominent midtropospheric trough just off the coast of Asia, and to extend about 10° longitude farther downstream toward North America.

While we expected that the variations in cyclone strength and track between the different simulations would have remote as well as local impacts through the mechanism of downstream development (e.g., Chang and Orlanski 1993), we were struck by the magnitudes illustrated in Figs. 15 and 16. By way of comparison, the simulations carried out by Torn and Hakim (2009) on the sensitivity of Tokage to initial conditions yielded standard deviations of ~70-m magnitude in the 500-hPa height from an ensemble of 48-h forecasts initialized at 1200 UTC 19 October. The ensemble of 10-day ECMWF forecasts analyzed by Anwender et al. (2008) indicated standard deviations in 500-hPa heights downstream of Tokage as

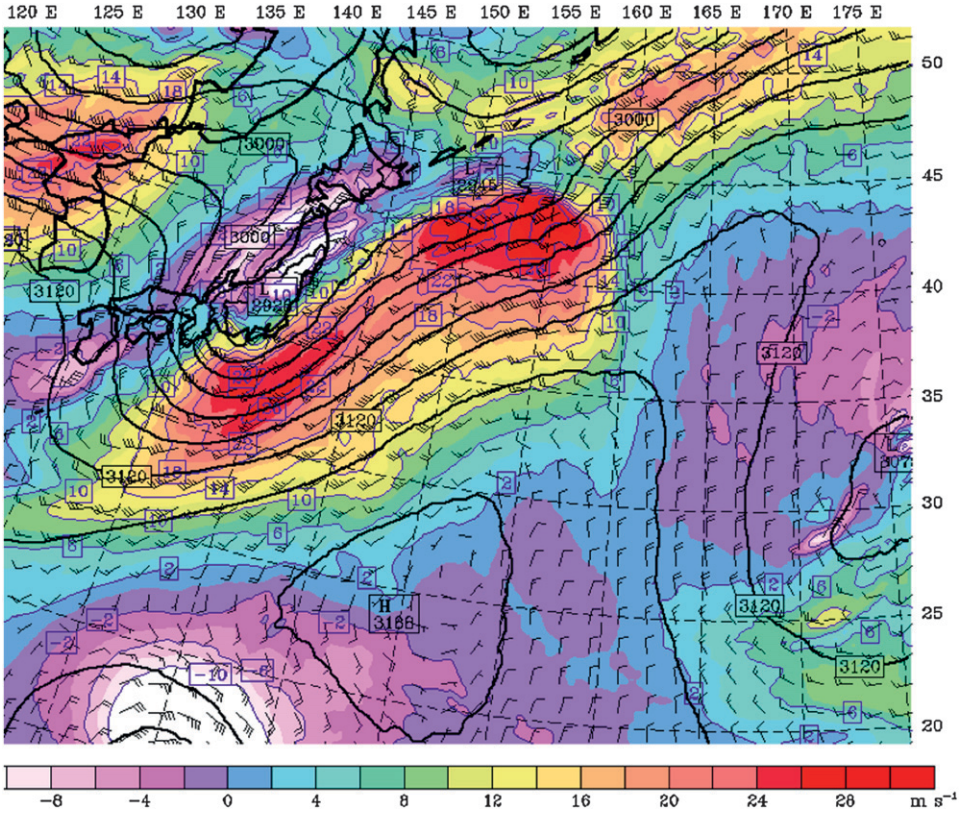

FIG. 11. Geopotential height (solid black lines; contour interval 30 m) and zonal wind speed (color fill; scale at bottom in m s^{-1}) on the 700-hPa surface at 0000 UTC 21 Oct 2004 from the warm SST perturbation simulation.

large as 100–120 m beginning about 23 October. They also found an anomalous trough–ridge–trough pattern for cases with enhanced intensification, which is consistent with the deviations from our cool SST simulation.

We conclude this section with a brief description of the results of the simulations for which the magnitude of the SST front at the Kuroshio Extension was enhanced and lessened by applying a zonally uniform sinusoidal perturbation of 1°C maximum amplitude with extrema at 30° and 40°N. These simulations yielded minor and inconsistent differences in storm structure after transition. Specifically, the strong and weak SST front simulations (not shown) yielded SLP minima on 0000 UTC 22 October that were 1 and 2 hPa lower than from the control simulation, respectively. There are also only modest differences between the simulations of atmospheric boundary layer temperatures for 21 and 22 October. The atmospheric boundary layer does not fully equilibrate to the underlying SST presumably because of the predominance of meridional flow before and during Tokage's passage. The results of Hart et al. (2006) suggest that if Tokage had taken a more zonal track, its transition would likely have been slower, and presumably it would be more responsive to the perturbations imposed in the SST front experiments.

5. Historical context

Our numerical experiments are for a single event, and hence the degree to which they are representative of the effects of SST perturbations on extratropical transitions in the western North Pacific in general is open to question. As a means of addressing this issue, we have carried out a retrospective analysis of the historical record, comparing the characteristics of these events during fall seasons with anomalously warm SST with those during periods of anomalously cool SST. We focus on the low-level meridional heat fluxes ($V'T'$) with these events. The character of these fluxes after the transition of Tokage is different in the warm SST simulation as compared with the cool SST simulation. The former includes relatively strong warm advection–meridional heat fluxes along a band well ahead (east to northeast) of the low pressure center, and the latter features these fluxes concentrated in a warm frontal zone extending from just north of the center toward the east-northeast. The meridional heat fluxes are

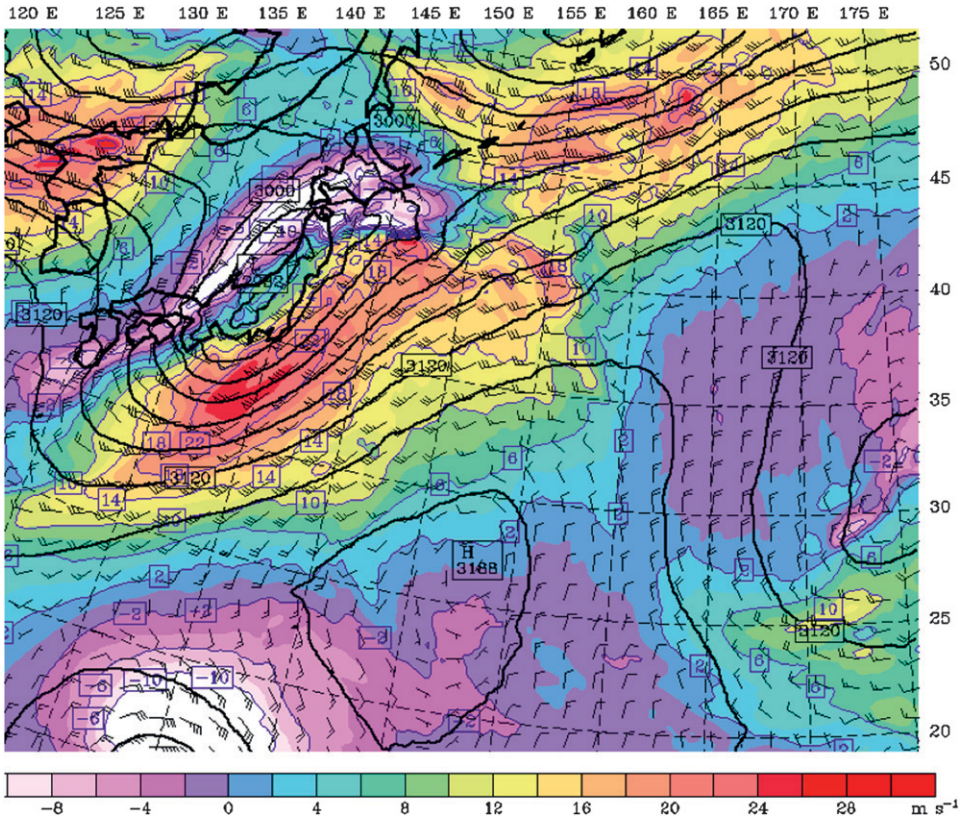

FIG. 12. As in Fig. 11, but for the cool SST perturbation simulation.

also a relevant parameter to consider in this comparison in that they represent an important aspect of the transient eddies (e.g., Lau 1978), specifically the vertical component of the Eliassen–Palm (EP) flux, with attendant implications on the forcing of the mean flow.

a. Methodology

The procedure used for this analysis was as follows. The warm and cold seasons [September–November (SON)] were selected on the basis of the average SST from the NCEP–National Center for Atmospheric Research (NCAR) reanalysis over a box extending from 29° to 41°N and from 135° to 155°E, as an approximation of the domain over which the perturbations were applied in our warm and cool SST simulations. Sets of years were constructed for which the mean SST was more than one standard deviation above, and less than one standard deviation below normal. Here 9 and 10 years were included in the warm and cool SST sets, respectively. The extratropical transitions during these years were catalogued using the best-track archive from the JTWC (available online at http://weather.unisys.com/hurricane/w_pacific/index.html). Selection was restricted to those events that propagated northward across 30°N between the longitudes of 125° and 155°E; a total of 40 and 45 storms were identified for the warm and cool years, respectively. Means and standard deviations in various properties of these events are itemized in Table 1. Note that the storms were a bit weaker on average during the periods of warm as compared with cool SST, but that these differences are modest. The meridional heat fluxes for these events were estimated using the NCEP–NCAR reanalysis. We generated high-pass-filtered gridded values of the meridional wind and air temperature at 850 hPa by applying a 3-day running mean twice and then subtracting the resulting smoothed time series of wind and temperature from the original series. Composite fields of $V'T'$ were then constructed for the 2 days following transition. These composites were formed in a storm-relative framework, with the $V'T'$ for each event shifted based on the displacement of the position of the surface low pressure center for the event from the mean position for the corresponding set of years. The timing for each event was based on the JTWC dataset. Since 2004 was not one of the warm or cool years, Tokage was not included in the retrospective analysis, but if it had, its contribution to the composite $V'T'$ would have been for the days of 21 and 22 October.

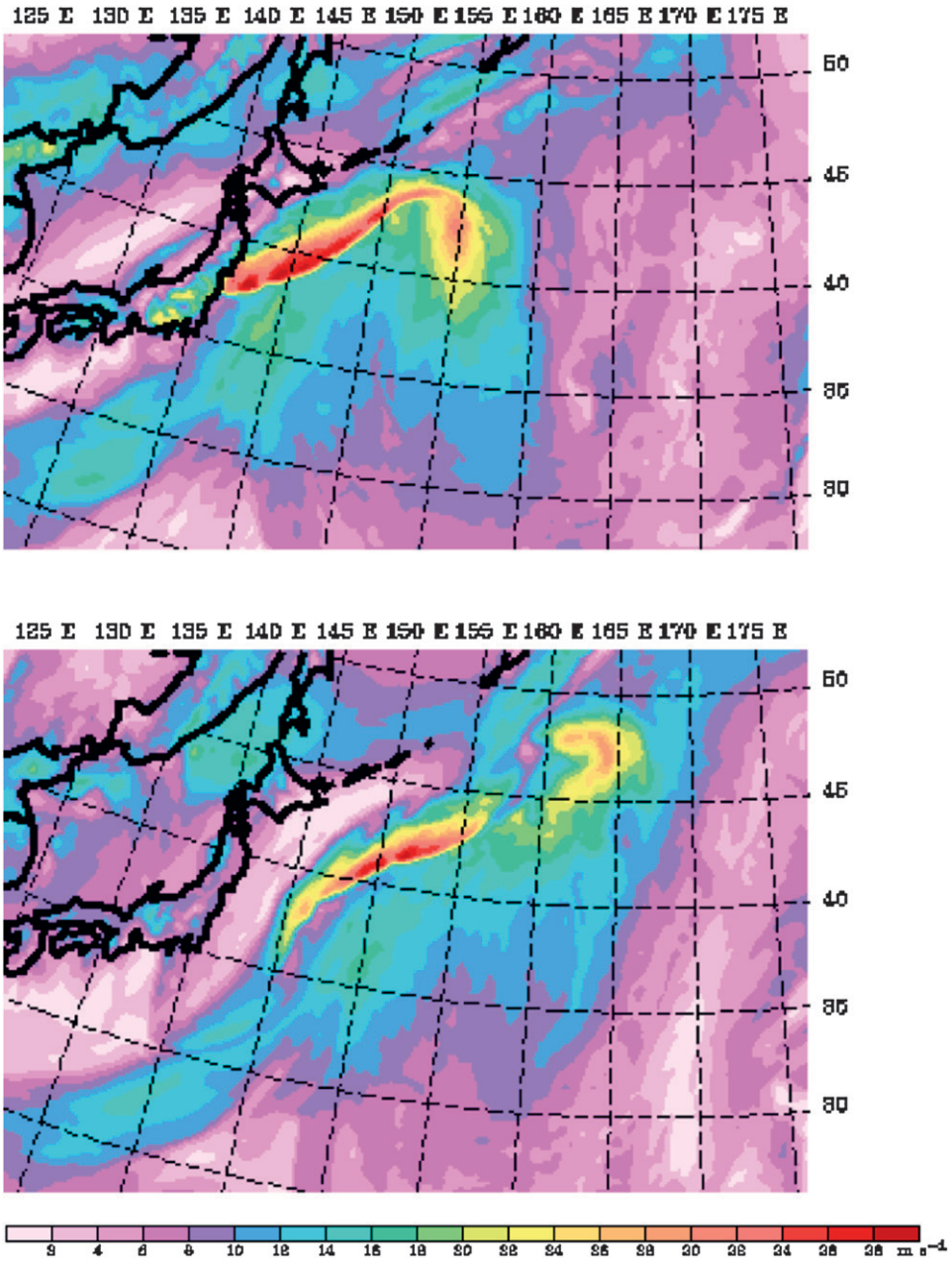

FIG. 13. Vertical wind shear (m s^{-1}) from the surface to 4 km at (top) 0000 UTC 21 Oct and (bottom) 1200 UTC 21 Oct 2004 from the warm SST perturbation simulation.

We recognize that the dataset used here has its limitations in terms of resolving derived quantities such as $V'T'$. As a check on its suitability, the SLP maps from the NCEP–NCAR reanalysis for individual events were examined. This survey indicated that a high proportion of the cases included distinct low pressure centers for the storms of interest early in their extratropical phase, suggesting that the reanalysis characterizes the lower-tropospheric structure in these situations reasonably well. A small fraction of the cases (10%–20%) in both the warm and cool SST years have only weak vestiges of a cyclonic circulation, apparently due to rapid weakening during their transition. These events were included in the composites. A more quantitative evaluation of the NCEP–NCAR reanalysis was carried out using the operational Pacific surface analyses from NCEP. These analyses were available for roughly the latest quarter of the events used in the composites. The mean central pressure for the

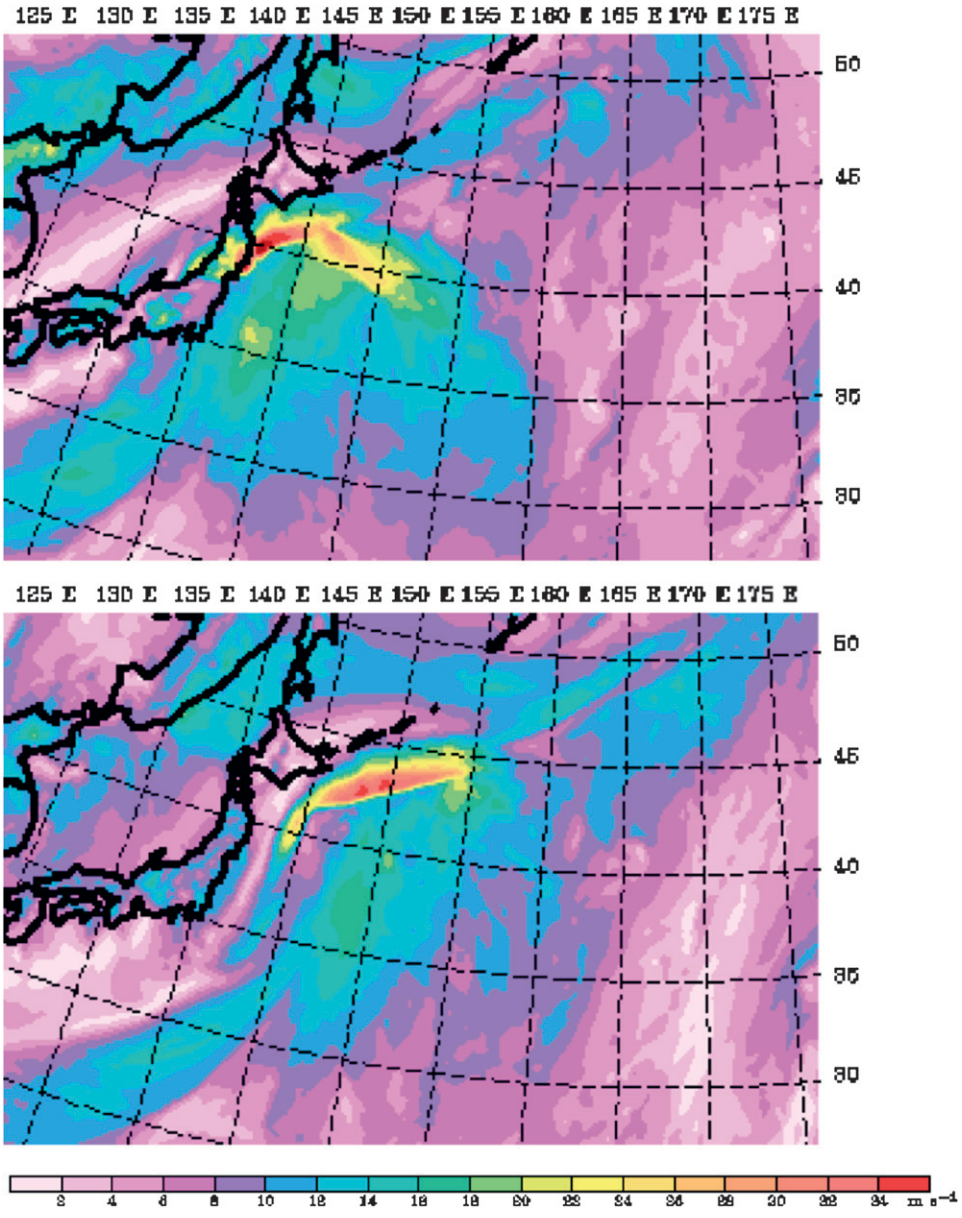

FIG. 14. As in Fig. 13, but for the cool SST perturbation simulation.

events at the end of their tropical phase, from warm and cool SST seasons combined, based on the operational analyses is 983 hPa; its counterpart based on the NCEP–NCAR reanalysis is 989 hPa. The individual values of minimum SLP from the two sources are strongly correlated ($r \sim 0.9$).

b. Composite results

The composite distribution of $V'T'$ for the events during years of anomalously warm SST is shown in Fig. 17. A maximum in $V'T'$ of 10 m s^{-1} °C is at 45°N, 160°E, which is roughly 800 km northeast of the mean location of the storms at the end of their tropical phase. The pattern of $V'T'$ includes a band of greater than 6 m s^{-1} °C centered near 45°N extending from the maximum to the date line. The corresponding distribution of $V'T'$ for the events during anomalously cold SST is shown in Fig. 18. The maximum meridional heat flux for this set of storms is 14 m s^{-1} °C, and is located about 500 km east-northeast of the mean position of the storms. Note that while relatively high values of $V'T'$ extend eastward from this maximum, as found for the warm years, the pattern for the cool years features a more pronounced bull's-eye in $V'T'$. For both the warm and cool SST composites, the

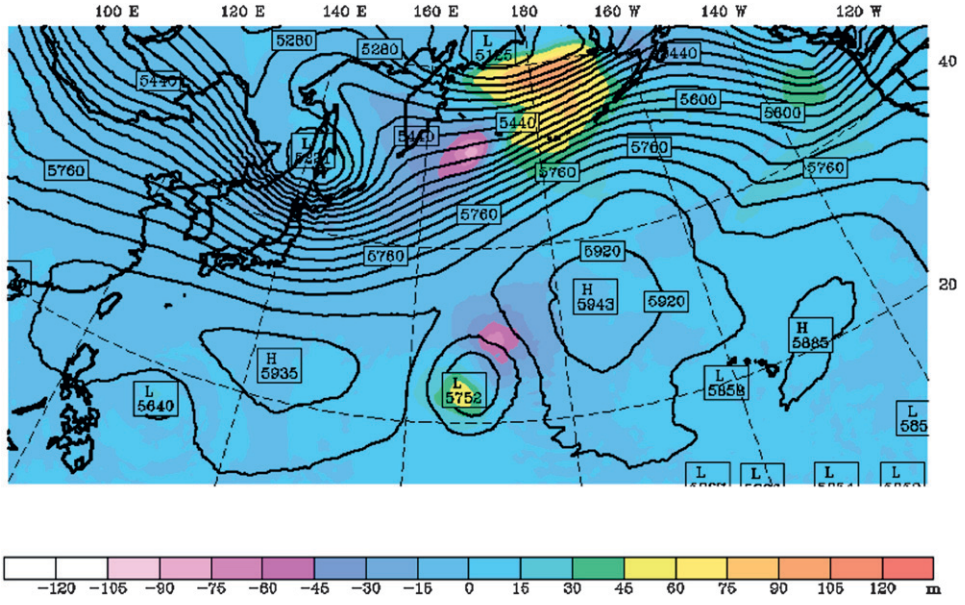

FIG. 15. Geopotential height of the 500-hPa surface (solid lines; contour interval 40 m) at 0000 UTC 23 Oct 2004 from the warm SST perturbation simulation. The color fill refers to the deviation in this height from the control simulation in the control minus perturbation sense (m; scale at bottom).

standard errors in the means in the region of the maximum $V'T'$ are ~2 m s^{-1} °C. From a Student's t-test perspective, the difference between the magnitudes of the $V'T'$ maxima is significant at the 90% confidence level.

We feel that these results are more intriguing than definitive. There are differences in the background circulation in the mean for the events during the two sets of years. For example, the westerly component of the 700-hPa flow is weaker for the warm SST events (Fig. 17) than for the cold SST events (Fig. 18). This difference is consistent with the slower eastward propagation of the storms in the warm years, and presumably has dynamical implications for development, especially in the post-tropical phases of these storms. Nonetheless, the meridional heat fluxes from the retrospective analysis bear at least some resemblance to our warm and cool SST simulations of Tokage. The warm SST simulation yielded moderate warm advection in a region well to the east and

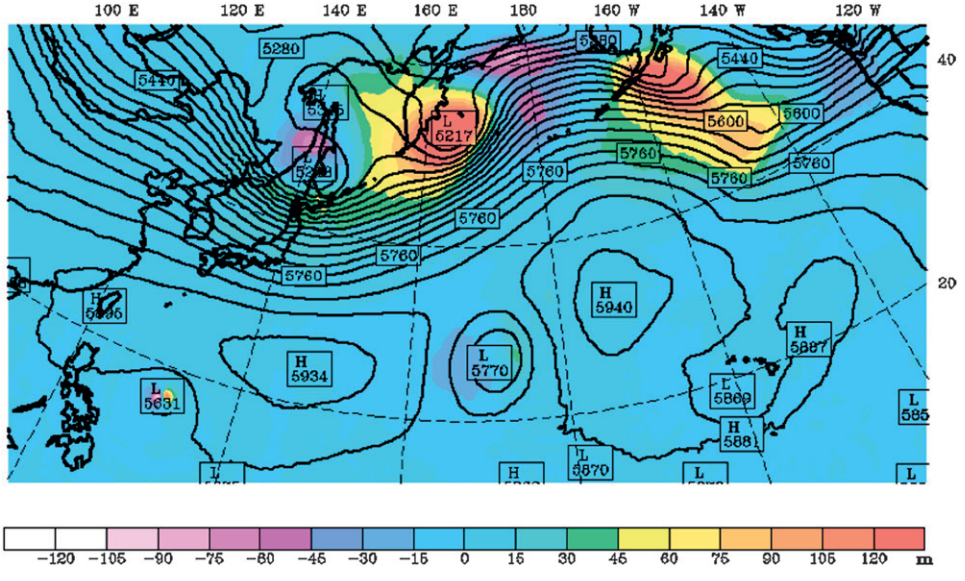

FIG. 16. As in Fig. 15, but for the cool SST perturbation simulation.

TABLE 1. Mean characteristics of transitions in seasons (SON) with warm and cool SST.

	Warm SST	Cool SST
No. of storms	40	45
Yr in composite	1955, 1961, 1977, 1979, 1990, 1994, 1998, 1999, 2000	1957, 1976, 1981, 1984, 1992, 1993, 1996, 1997, 2002, 2006
Avg date at 30°N	3 Oct	7 Oct
Avg °E lon at 30°N	137.4 ± 8.0	142.0 ±7.3
Avg max winds at 30°N (kt)	71 ± 19.9	77 ± 21.2
Avg °N lat at end of transition	42.0 ± 6.8	40.7 ± 6.0
Avg °E lon at end of transition	150.5 ± 13.3	160.1 ± 13.7

northeast of the low center, while the cool SST simulation yielded intense warm advection concentrated along a strong warm front extending east-northeastward from near the low center itself.

6. Summary and discussion

A series of high-resolution simulations with WRF have been carried out to investigate the effects of regional SST perturbations on extratropical transition in the western North Pacific, using Typhoon Tokage as a case study. These simulations indicate substantial atmospheric sensitivity to broadscale perturbations in SST of order 1°–1.5°C. An intriguing result is that the simulation with the negative (cool) perturbation in SST that yields the strongest storm about 2 days after transition. The enhanced development in this situation is associated with a less eastward track of the low-level circulation center, which then is more favorably phased with an approaching upper-level trough. This simulation also features a relatively strong warm front; it is unclear the degree to which it is more a cause versus an effect of cyclogenesis. This ambiguity is caused by the imposed SST perturbations, as manifested through the surface fluxes of sensible and latent heat, which induces changes in both the track and the lower-tropospheric thermal structure of the storm. These changes, while initially small, are subject to internal dynamics and feedbacks that result in profound differences in the storm's simulated evolution over an interval of only 24 h.

We acknowledge that the results of our numerical experiments are tentative, in that they are based on a single case. In addition, Tokage may represent a case of enhanced atmospheric sensitivity. The numerical experiments of Torn and Hakim (2009) indicate considerably greater sensitivity to initial conditions for Tokage relative to another western North Pacific typhoon (Typhoon Nabi) undergoing transition. The uncertainty in the applicability of our findings for Tokage to extratropical transitions in general motivated us to complement our simulations with a retrospective analysis.

The retrospective analysis used the NCEP–NCAR reanalysis to examine past western North Pacific transitions.

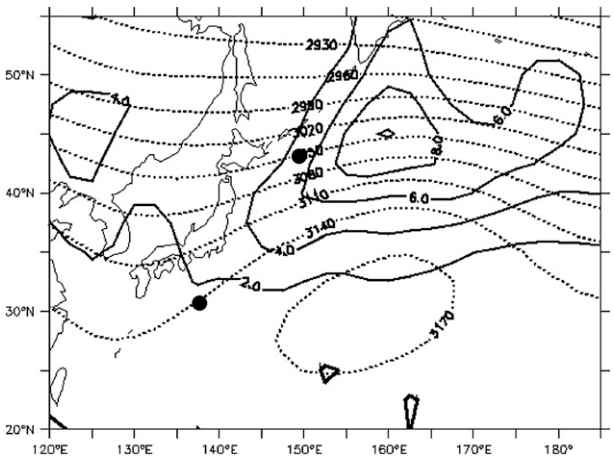

FIG. 17. Distribution of $V'T'$ (solid lines; contour interval 2 m s^{-1} °C), and mean 700-hPa geopotential height (dashed lines; contour interval 30 m) for the extratropical transitions during the fall seasons (SON) with positive SST anomalies. The large dots indicated the mean longitude at which the storms crossed 30°N and the mean latitude and longitude at the end of their transitions. See text for details.

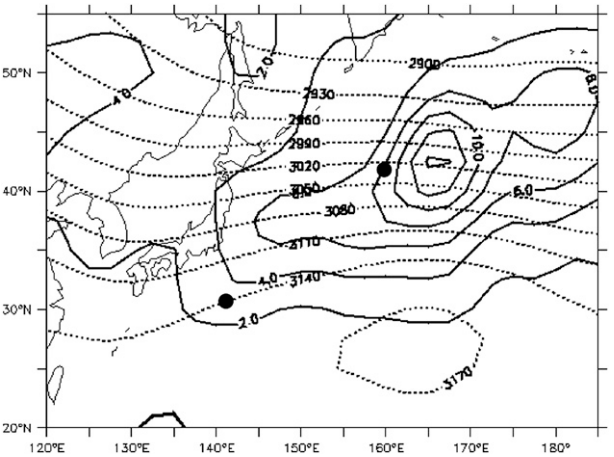

FIG. 18. As in Fig. 17, but for the fall seasons with anomalously cool SST.

We considered separately seasons (SON) with anomalously warm and cold SST in the region for which the broadscale perturbations were prescribed in our simulations. The pattern of mean meridional heat fluxes ($V'T'$) during the seasons of warm SST includes a broad maximum well east of the mean location of the storm centers, while the corresponding pattern during the seasons of cool SST features a stronger and better-defined maximum in closer proximity to the storm centers in the mean. While the differences between these patterns are broadly consistent with the results from the warm and cool SST perturbation simulations, the weaker westerlies aloft for the set of events during the seasons of warm SST versus that for the cool SST set may represent an important, confounding factor.

The impacts associated with changes in SST will depend on the synoptic environment encountered by a storm as it is undergoing transition. The composite results of Hart et al. (2006) regarding post-transition storm intensity versus SST gradient indicate that these impacts may even often act in the opposite sense than found here. Regardless of the applicability of our results for Tokage to extratropical transitions in general, they do indicate that in these situations the atmosphere in a western boundary current region can be quite sensitive to SST perturbations of the magnitude and spatial scale of observed seasonal and longer-term anomalies.

We hope this paper encourages follow-up studies of the potential influences of SST in other situations and locations. Our numerical results may have depended on the boundary layer parameterizations of the surface fluxes and mixing that were employed. Analysis of the sensitivity of the model results to the boundary layer scheme is outside the scope of the present paper but might be a fruitful topic for further research.

There are large differences in the 500-hPa flow between the control, warm, and cool SST simulations after transition. Torn (2010) stressed the importance of the distribution and magnitude of low-level moisture advection to ridging aloft in numerical experiments on Tokage; notable differences in the nature of the poleward flow to the east of the surface low center are also indicated in the simulations for the present paper. It bears emphasizing that the consequences are not limited to the vicinity of the storm itself, but also propagate, especially downstream. Therefore, these kinds of disturbances may tend to be responsible for a disproportionately large source of variability for the hemispheric circulation at this time of year. Moreover, they appear to represent a special challenge for NWP, as exemplified in Fig. 8 of Jones et al. 2003. The present results suggest that additional research may be warranted on the air–sea interactions in NWP models during extratropical transition, and in particular whether errors in accounting for these interactions constitute a significant source of unpredictability.

Acknowledgments. We appreciate the thorough and insightful reviews provided by three anonymous reviewers. Support for this research was provided by NOAA's Office of Global Programs CLIVAR Program. This publication is partially funded by the Joint Institute for the Study of the Atmosphere and Ocean (JISAO) under NOAA Cooperative Agreement NA17RJ1232.

REFERENCES

Anwender, D., P. A. Harr, and S. C. Jones, 2008: Predictability associated with the downstream impacts of the extratropical transition of tropical cyclones: Case studies. *Mon. Wea. Rev.,* **136,** 3226–3247.

Bond, N. A., and D. E. Harrison, 2000: The Pacific Decadal Oscillation, air-sea interaction, and central North Pacific winter atmospheric regimes. *Geophys. Res. Lett.,* **27,** 731–734.

Bosart, L. F., and G. M. Lackmann, 1995: Postlandfall tropical cyclone reintensification in a weakly baroclinic environment: A case study of Hurricane David (September 1979). *Mon. Wea. Rev.,* **123,** 3268–3291.

Chan, J. C., 2005: Interannual and interdecadal variations of tropical cyclone activity over the western North Pacific. *Meteor. Atmos. Phys.,* **89,** 143–152.

Chang, E. K. M., and I. Orlanski, 1993: On the dynamics of a storm track. *J. Atmos. Sci.,* **50,** 999–1015.

Davis, C., and Coauthors, 2008: Prediction of landfalling hurricanes with the Advanced Hurricane WRF model. *Mon. Wea. Rev.,* **136,** 1990–2005.

Emanuel, K. A., 1986: An air–sea interaction theory for tropical cyclones. Part I: Steady-state maintenance. *J. Atmos. Sci.,* **43,** 585–605.

Evans, J. L., and R. E. Hart, 2003: Objective indicators of the onset and completion of ET for Atlantic tropical cyclones: Factors determining post-transition evolution. *Mon. Wea. Rev.,* **131,** 909–925.

Harr, P. A., and R. L. Elsberry, 2000: Extratropical transition of tropical cyclones over the western North Pacific. Part I: Evolution of structural characteristics during the transition process. *Mon. Wea. Rev.,* **128,** 2613–2633.

Hart, R. E., 2003: A cyclone phase space derived from thermal wind and thermal asymmetry. *Mon. Wea. Rev.,* **131,** 585–616.

——, and J. L. Evans, 2001: A climatology of the extratropical transition of Atlantic tropical cyclones. *J. Climate,* **14,** 546–564.

——, ——, and C. Evans, 2006: Synoptic composites of the extratropical transition life cycle of North Atlantic tropical cyclones: Factors determining post-transition evolution. *Mon. Wea. Rev.,* **134,** 553–578.

Jones, S. C., and Coauthors, 2003: The extratropical transition of tropical cyclones: Forecast challenges, current understanding, and future directions. *Wea. Forecasting,* **18,** 1052–1092.

Klein, P. M., P. A. Harr, and R. L. Elsberry, 2000: Extratropical transition of western North Pacific tropical cyclones: An overview and conceptual model of the transformation stage. *Wea. Forecasting,* **15,** 373–395.

Kushnir, Y., W. A. Robinson, I. Blade, N. M. J. Hall, S. Peng, and R. Sutton, 2002: Atmospheric GCM response to extratropical

SST anomalies: Synthesis and evaluation. *J. Climate,* **15,** 2233–2256.

Lau, N.-C., 1978: On the three-dimensional structure of the observed transient eddy statistics of the Northern Hemisphere wintertime circulation. *J. Atmos. Sci.,* **35,** 1900–1923.

Mantua, N. J., S. R. Hare, Y. Zhang, J. M. Wallace, and R. C. Francis, 1997: A Pacific interdecadal climate oscillation with impacts on salmon production. *Bull. Amer. Meteor. Soc.,* **78,** 1069–1079.

Minobe, S., A. Kuwano-Yoshida, N. Komori, S.-P. Xie, and R. J. Small, 2008: Influence of the Gulf Stream on the troposphere. *Nature,* **452,** 206–209, doi:10.1038/nature06690.

Nakamura, H., T. Sampe, Y. Tanimoto, and A. Shimpo, 2004: Observed associations among storm tracks, jet streams and mid-latitude oceanic fronts. *Earth's Climate: The Ocean–Atmosphere Interaction, Geophys. Monogr.,* Vol. 147, Amer. Geophys. Union, 329–345.

Nonaka, M., and S.-P. Xie, 2003: Covariations of sea surface temperature and wind over the Kuroshio and its extension: Evidence for ocean-to-atmospheric feedback. *J. Climate,* **16,** 1404–1413.

Peng, S., W. A. Robinson, and M. P. Hoerling, 1997: The modeled response to midlatitude SST anomalies and its dependence on background circulation states. *J. Climate,* **10,** 971–987.

Skamarock, W. C., and Coauthors, 2008: A description of the advanced research WRF version 3. NCAR Tech. Note NCAR/TN-475+STR, 125 pp. [Available online at http://www.mmm.ucar.edu/people/skamarock/.]

Sutcliffe, R. C., and A. G. Forsdyke, 1950: The theory and use of upper air thickness patterns in forecasting. *Quart. J. Roy. Meteor. Soc.,* **76,** 189–217.

Tokinaga, H., and Coauthors, 2006: Atmospheric sounding over the winter Kuroshio Extension: Effects of surface stability on atmospheric boundary layer structure. *Geophys. Res. Lett.,* **33,** L04703, doi:10.1029/2005GL025102.

——, Y. Tanimoto, S.-P. Xie, T. Sampe, H. Tomita, and H. Ichikawa, 2009: Ocean frontal effects of the vertical development of clouds over the western North Pacific: In situ and satellite observations. *J. Climate,* **22,** 4241–4260.

Torn, R. D., 2010: Diagnosis of the downstream ridging associated with extratropical transition using short-term ensemble forecasts. *J. Atmos. Sci.,* **67,** 817–833.

——, and G. J. Hakim, 2009: Initial condition sensitivity of western Pacific extratropical transitions determined using ensemble-based sensitivity analysis. *Mon. Wea. Rev.,* **137,** 3388–3406.